Chapter V

Raman characteristics of Eu^{3+}:$GdVO_4$ nanosystems

Raman spectroscopy is an effective analytical tool for probing the solid state structure of crystals as it is subtly sensitive to the manifestation of dopants/impurities, and crystal defects in the host lattice. Any disturbance in the general crystalline symmetry upon inclusion of dopants/ impurities thereby affects the lattice vibrational modes of the host crystal. Of all the laser host materials known to us, Yttrium, gadolinium, and calcium orthovanadate crystals are recognized as the most effective ones and has gained considerable attention [1, 2]. Gd based orthovandate crystals display much higher absorption coefficient properties, high thermal conductivity as well as larger emission cross-section as compared to Y based crystals, proving them to be better lasing host materials amongst the well-studied orthovanadates [3, 4]. These orthovanadate crystals can also be used as the active materials for stimulated Raman scattering (SRS). In $GdVO_4$ system, the most intense mode observed is usually the high frequency $\nu 1$~882 cm^{-1} corresponding to V-O stretching (symmetric) internal vibration in the tetrahedral $(VO_4)^{3-}$ anionic group [5]. For self-Raman lasing activity, this high frequency Raman mode has been considered to be most effective [6]. The other important Raman mode, although weak, observed in such crystals $\nu 2$ ~380 cm^{-1} corresponds to the O-V-O bending mode [3]. Recent reports can be found in literature that effectively utilized the low frequency mode for self-Raman lasing [7]. This line is relatively broader than the other modes observed considering overlap of two symmetric bending (scissoring and twisting) modes (A_g + B_g) of internal vibrations of the tetrahedral $[VO_4]^{3-}$ group [8].

Reports can be found that deal with discussions on zircon-type $REVO_4$ system displaying various polymorphs undergoing phase transitions to a tetragonal scheelite-type structure under high pressure [9, 10]. However, such phase transitions are studied considering the high frequency Raman modes. In the low frequency regime temperature dependent inhomogeneous splitting of the low frequency $\nu 2$ vibrational lines has been assigned to structural disordering caused in the crystal lattice [11]. Interestingly the line is asymmetrical and is composed of two modes. One of which is temperature dependent characteristic of scheelite

type structure and is non-zero even at room temperature [10]. So far we have not come across any report that deals with valuable information on the effect of dopant inclusion in the $\nu 2$ raman mode. In the present work, we try to observe effect of dopant concentration on the nature of the low frequency ~ $\nu 2$ raman mode following detection of shifting, change in intensity and broadening of Raman bands of the host crystal.

5.1. Experimental details:

Raman study employing a Renishaw In-Via Raman spectrometer (Make: Renishaw, Wottonunder- Edge, UK) and using the 514.5 nm line of Ar^+ laser as the excitation source were performed on samples prepared as described in Chapter II.

5.2. Results and discussion:

5.2.1. Detection and analysis of active Raman modes

Analysis of group theory regarding vibrations in the zircon type crystal structure with space group D_{4h}^{19} and two formula units in the unit cell gives the following vibration spectrum composed of two sublattices of RE cationic and $[VO_4]^{3-}$ anionic, decomposed in the terms of the irreducible representations [12, 13].

$$\Gamma = 2A_{1g} + A_g + 4B_{1g} + B_{2g} + 5E_g + A_{1u} + 4A_{2u} + B_{1u} + 2B_{2u} + 5E_u \quad (5)$$

The Raman active modes observable, marked in bold in above Eq. (5) can thence be elaborated as:

$$\Gamma = A_{1g}(\nu_1, \nu_2) + B_{1g}(2T, + \nu_3, \nu_4) + B_{2g}(\nu_2) + E_g(2T, R, \nu_3, \nu_4) \quad (6)$$

In Eq. (6) ν_i (i = 1,…, 4) correspond to four internal vibrational modes (symmetric and asymmetric stretching and bending) of the VO_4^{3-} tetrahedron and T, R corresponds, to the translational or rotational motion respectively [14].

Of the observable 12 Raman active modes at the center of the Brillouin zone, modes observed in our study (**FIGURE 1 (A)),** in the region 260-1000 cm^{-1} are internal stretching and bending vibrations of the tetrahedral group while the

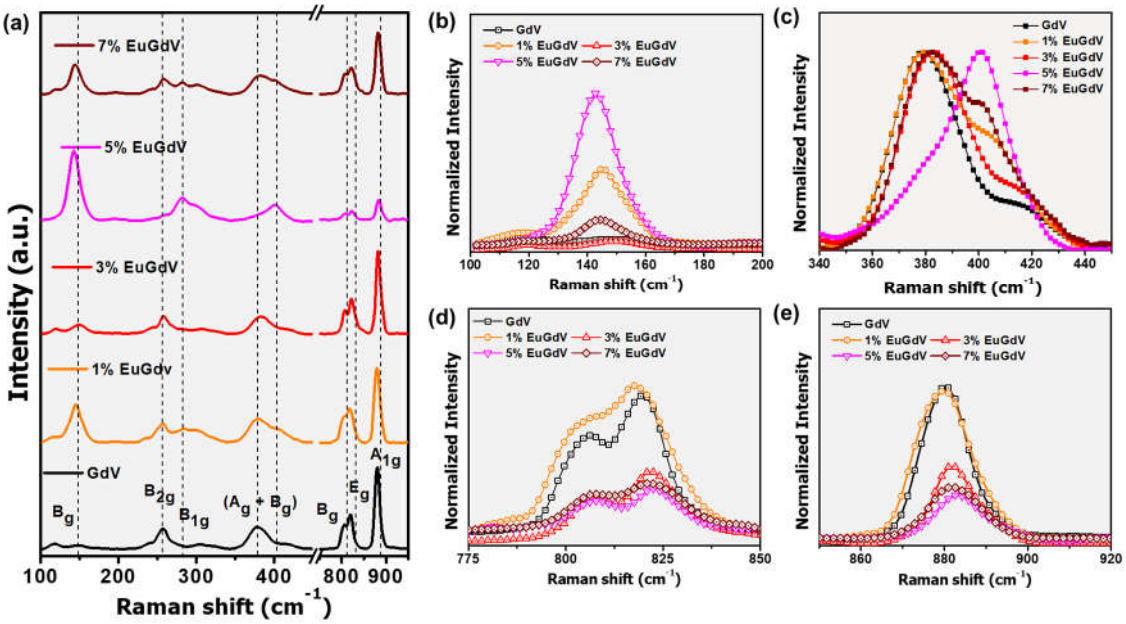

FIGURE 5.1: Raman shift observed for the various doped samples is shown in (a). Normalized Raman spectra displaying significant modes in various ranges are displayed in (b-e).

modes observed at 100-250 cm^{-1} are external ones and are in good agreement with the reported literature [14-16]. B_{2g} translatory vibrational (asymmetrical) mode, observed at ~258 cm^{-1} represents the Eu–O stretching while A_{1g} corresponds to O-V-O vibration. Gd-O stretching. The most intense Raman mode observed in our case as shown in **FIGURE 5.1 (a)** is the high-frequency $\nu 1$ = 880 cm^{-1}, corresponding to vibrational structure (stretching internal vibration in the tetrahedral $[VO_4]^{3-}$ anionic group) for an ideal tetragonal zircon-type structure ($I4_1/amd$) [5, 17-19].

The only anomaly observed was in the case of 5% EuGdV where the most intense peak was centered at ~143 cm^{-1}, which is elaborated in **FIGURE 1 (b**). This peak supposedly originates due to B_g(IV) of fergusonite structure and in some reports is also attributed to the presence of V_2O_5 probably caused by some partial decomposition [11, 20]. Moreover, the signal can be ascribed to external mode T-like vibrations, corresponding to Gd-O stretching [14, 15]. Since XRD results do not display any signal arising due to presence of unreacted V_2O_5, the latter

Table 5.1: Assignment of various Raman modes observed

Shift (cm^{-1})	Modes assigned
260-1000	Internal stretching and bending vibrations of the tetrahedra
258	B_{2g} translatory vibrational (asymmetrical) mode Eu–O stretching
257	Gd-O stretching
143	T-like vibrations, corresponding to Gd-O stretching
ν2 ~380	Symmetric V-O stretching or O-V-O bending model
ν3 modes ~800-820	Overlap of two E_g and B_{1g} modes.
ν1 mode ~880	Vibrational structure (stretching internal vibration in $[VO_4]^{3-}$ anionic group)

explanation for the origin of the peak is more appropriate. Presence of external mode signals in Eu^{3+} doped GdVO4 system can be confirmed from existing literature [21]. We also observed secondary Raman modes ~257 (Gd-O stretching) [22]. The other significant peak observed is the low-frequency (bending mode) Raman line $\nu 2$ ~380 cm^{-1} for $GdVO_4$ symmetric V-O stretching or O-V-O bending mode1 [7]. It is known that the $[VO_4]^{3-}$ anionic group in zircon type crystal structure vanadates exists in the form of isolated tetrahedra [23]. This anionic group provides such strong covalent bonds that they may as well be treated as individual structural elements, and thus their internal vibrations observed in. Raman spectra reveals information on the structural ordering of the crystal system; distortions in the lattices to be more specific [11]. The symmetric $\nu 1(A1)$

vibration is a singlet, while $\nu 2(E)$, $\nu\ 3(F2)$, and $\nu 4(F2)$ modes are in general recorded as doublets [11]. The $\nu 3$ modes are detected ~800-820 cm^{-1} and are viewed to be an overlap of two E_g and B_{1g} modes.

The normalized raman spectra can be found in **FIGURE 1 (b-e).** Interestingly upon doping, B_{1g} mode gains intensity, to be highest as in case of 5% doped sample **((FIGURE 1(b)).** Upon normalization we observe that the signal at ~380 cm^{-1} (O-V-O bending mode) signal had the paramount effect of Eu^{3+} dopant

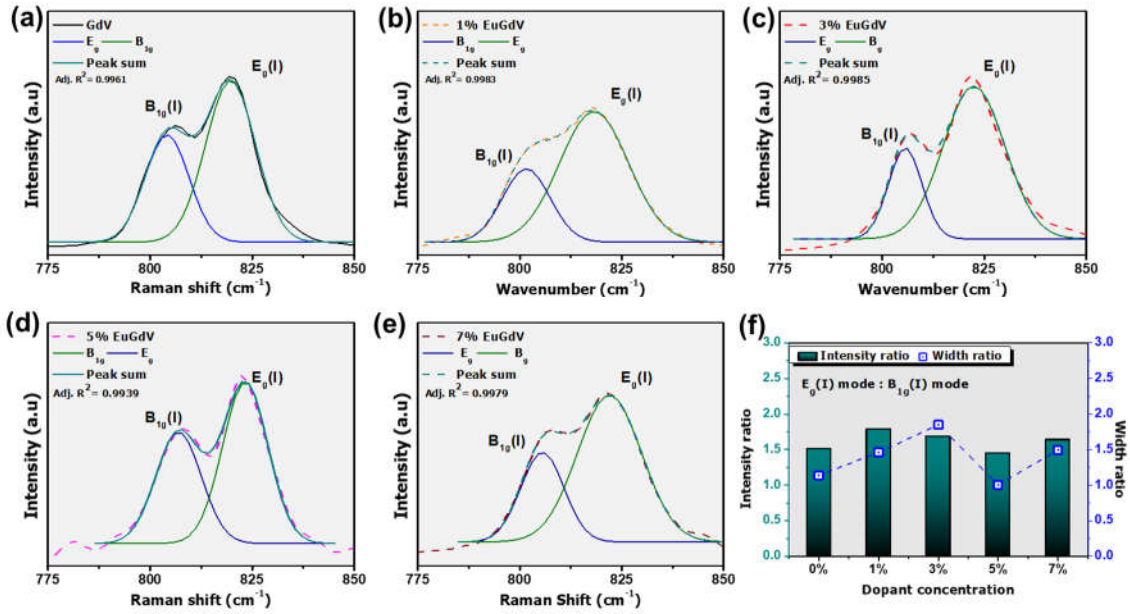

FIGURE 5.2: Raman spectra for as prepared samples displaying deconvoluted ν3 mode showing overlap of Bg(I) and Eg(I) modes for (a) GdV, (b) 1% EuGdV, (c) 3% EuGdV, (d) 5% EuGdV and (e) 7% EuGdV respectively. (f) displays the plot for intensity and width ratio of the two components ibserved in ν3 mode.

concentration with the spectra displaying more complex and asymmetrical as well as broader profile when dopant concentration was increased (Figure 1(c)). The $\nu 3$ modes i.e. E_g and B_{1g} observed in our study maintained their profile without much changes, as can be seen in **FIGURE 5.2**. Minimal effect of doping was observed while the width ratio between E_g and B_{1g} being the highest for 3% EuGdV (**FIGURE 5.2. (b)**). As for the $\nu 3$ and $\nu 1$ mode, the observations were similar with decrement of intensity beyond 3% dopant concentration. Only a limited number

of reports can be found in literature that discuss the effect of dopants on the Raman spectra of a nanosystem. Pal *et al.* reported that increment in Eu^{3+} dopant concentration influences the vibrational properties of host to a great extent such that the intensities of Raman mode decreases drastically [24]. D. Tuschel reported the effect of RE doping in ABO_4 system and observed asymmetry induced due to inclusion of dopant [25]. Ningthoujam, R.S. *et al.* reported weakening of intensity of Raman modes in Eu^{3+} doped $GdVO_4$ nanosystem as a function of Eu^{3+} concentration increase from 2% to 5% [26]. While discussing the effect of dopant concentration, the most important aspect of concern is the site occupancy of the dopant ion. In our study, Eu^{3+} is supposed to substitute Gd^{3+} sites due to closer ionic sizes. However, occupancy of defect sites cannot be overlooked. Both the features are effected by a great deal with variation in dopant concentration and hence the dissimilarity in the facets of Raman spectra observed. Incorporation of dopant disrupts the long-range translational symmetry at a crystal lattice site which in turn is responsible for rise in the distribution of phonon energy states, thus effecting the Raman bands [25]. Another important observation is that not all modes are affected equally, by virtue of heterogeneity induced in the crystal due to Eu^{3+} inclusion. It is known that active lattice vibrational modes, which consists of substantial contribution of atomic motion from the substituted atom, demonstrates the most significant variation in spectra [25].

5.2.2. Zircon-scheelite partial phase transition

Raman spectra profiling of the asymmetric A_{1g}(II) vibration line, caused due to ν2(E) internal vibration splitting of the free tetrahedral anionic group by strong RE matrix crystal field, can be observed in **FIGURE 5.3**. Upon deconvolution our observations suggest presence of strong overlap of two bending modes (A_{1g} and B_{2g}). Such an overlap is characteristic of partial scheelite type structures and although similar in many respects, an ideal zircon structure does not reveal any such overlap [6, 11]. Researchers have tried to explain this nature, with emphasis on existence of intermediate minima for a rotation of molecular units at a certain angle with respect to their regular sites [27, 28].

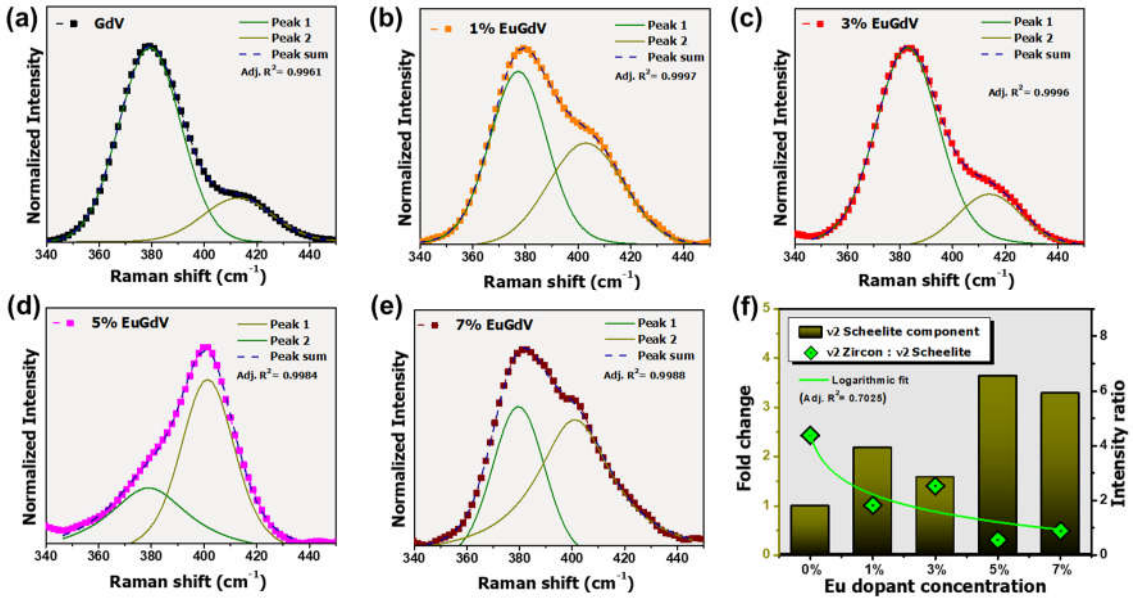

FIGURE 5.3. Deconvoluted (Ag+Bg) overlap ν2 mode displaying the zircon type (green line) and structural disordering dependent scheelite type component (yellow line) for GdV, 1% EuGdV, 3% EuGdV, 5% EuGdV and 7% EuGdV respectively (g-k).

Observation of such an overlap, as in this case, confirms existence of aforementioned intermediate minima for a rotation of molecular units, in this case the anionic tetrahedral [27]. Such partial zircon–scheelite phase transition has been previously reported following thermally activated rotation by 45° of few tetrahedral anionic groups whereby the additional component in the $\nu 2$ Raman line can be identified as the scheelite-type internal vibration [11]. Existence and occupancy of irregular sites of the tetrahedral anion $[VO_4]^{3-}$ can lead to shifting and widening observed with respect to one another, thereby manifesting the observance of splitting due to different crystal field in case of different dopant concentration (**FIGURE 5.3**). We speculate that inhomogeneous structural disordering as a consequence of irregular incorporation of Eu(III) into irregular sites of the vanadate matrix lead to the line widening as well as intensity gain of the scheelite component as observed in our study [29]. Furthermore, the asymmetry in the band induced due to the Eu-doping describes that the lattice structure of the partially transitioned doped samples are under stress [30, 31].

Various zircon peaks are likely to overlap with those of the scheelite character and therefore, XRD diffractogram refinement does not give accurate lattice

parameters [10]. Cases of partial or secondary phases in tetragonal crystal structures thus are difficult to be determined from XRD analysis. In this scenario, importance of Raman spectroscopic analysis grows as it has been proven to be an efficient way to detect spurious phases even for relatively very low concentrations which are in general almost undetectable by means X-ray diffraction technique [31, 32]. Importantly, tetragonal scheelite type structures have a space group of $I4_1/a$ which is a subgroup of zircon type tetragonal system with a space group of $I4_1/amd$ [33]. The zircon a-axis is ~√2 times diagonal that of scheelite-type unit-cell and hence lattice structure of both crystal types are similar per se. Furthermore, in both the lattice types the tetrahedral group and the dodecahedral group are found to be interconnected in a comparable manner which can be interpenetrated as diamond-like lattices if we consider "deoxygenated" structures [34]. However, the scheelite *c*-parameter is double than that of the zircon unit cell and has volume contraction of ~10% [10]. It can thus be established that the zircon-scheelite transitions are first-order non-reversible transitions [33, 35]. A possible mechanism of the transition has been described which involves two processes which may occur simultaneously as well: (1) Increment of density by ~10% leading to simple shearing of the zircon-type structure and (2) relative displacement of atoms [36].

The structure converts to a quasi scheelite-type structure in the first process itself and is achieved by readjustments of the site symmetries. In such processes, the [110] direction of zircon becomes the [100] direction of scheelite, whereas [001] direction is shared however the c-axis for scheelite is twice as elongated. We attempted to illustrate the mechanism involved with a graphical representation for the unit cell transition from zircon to scheelite type crystal in Figure 5.4. The unit cells are prepared using Vesta® following information available from XRD analysis of the sample. Note that the orientations in the figure are projections along the *hkl* planes undergoing transformations upon dopant induced structural disorder. Interestingly, the most drastic change in such transitions from zircon to scheelite type, is observed in the difference of bond angles, specifically ∠Gd-V-O

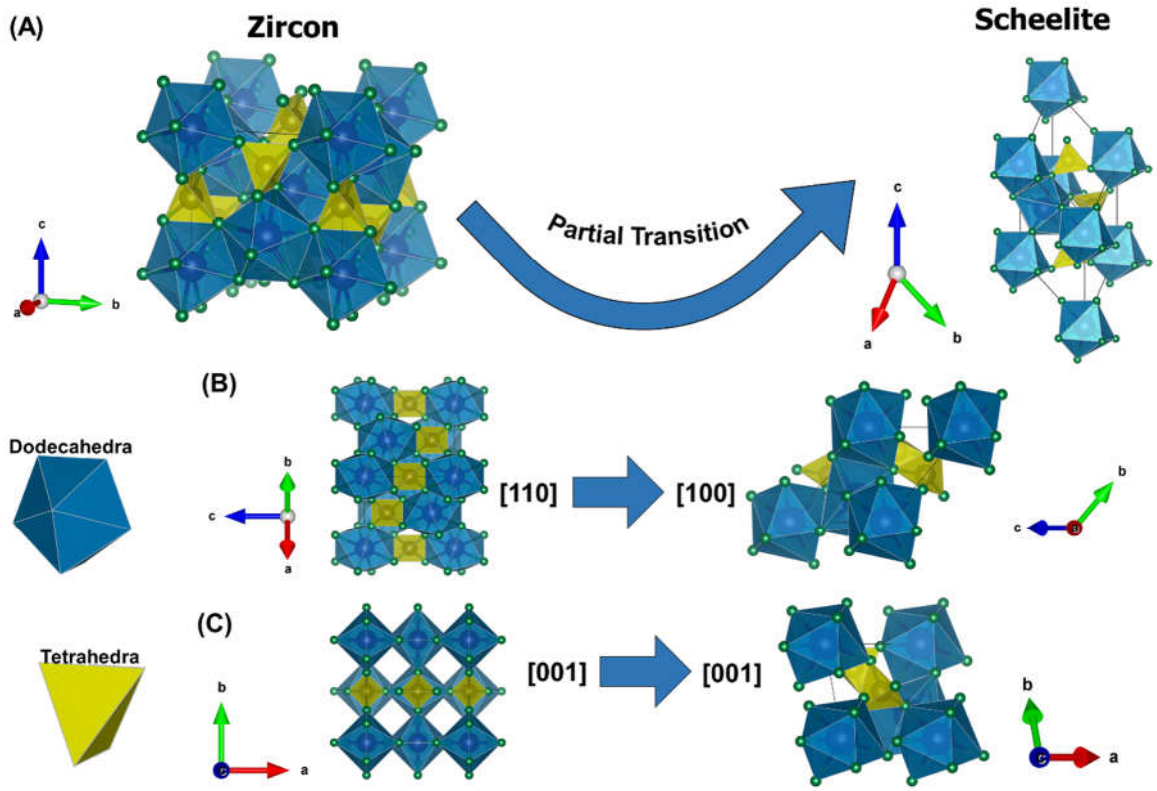

Figure 5.4: Unit cells are prepared using Vesta® demonstrating (A) transition from Zircon to scheelite. display change in orientations for projections along the hkl planes B) [110] to [100] and (C) [001] sharing by the two lattice types.

and ∠Gd-O-Gd [35]. It is worth mentioning that Gd-V-O interact via interlinking of two different groups: free tetrahedral for V-O and dodecahedra for Gd-O. Thus two different bond length of ∠Gd-V-O exists in the system which can be effected upon inclusion of dopants significantly. Although such transitions in AVO_4 nanosystem are at large associated with alterations due to high pressure and temperature variation, the correlation of the internal vibrations of free tetrahedra $[VO_4]^{3-}$ groups with of their local symmetries and the crystal factor needs to be emphasized upon [11]. $GdVO_4$ crystal with a larger cation, displays comparable scheelite-type and zircon-type component intensities even at room temperature, and the occurrence of the scheelite-type component can be attributed to originate from structural disordering in the lattice system [6]. Thus in case of $GdVO_4$ crystal, the scheelite component need not be induced by pressure or temperature and can

be observed at ambient conditions. It can be observed in Figure 5.3 (f) that the asymmetry profile fluctuates with increment in the scheelite-type component as dopant concentration was increased. Meanwhile, the intensity ratio for zircon to scheelite-type component is observed to be following a decreasing trend. The best-fit curved line for the observation made is a logarithmic trend suggesting that the rate of variation in the component decreases quickly and then levels out as Eu incorporation was increased. It is noteworthy that the incorporation of dopants into the system can only effect the local symmetry of the site occupied by the dopant ion. Since the dopant concentration is below 10%, only a fraction of unit cells undergo transition and hence the scheelite phase is not prominently deliberated in other studies except for the low frequency ν2 mode of Raman spectra. We conclude in terms of crystal lattice both the zircon and scheelite type lattice structures, containing indistinguishable tetrahedral cation sublattices, undergo transformation (from zircon to scheelite lattice type) following change in bond angles via rotation of the tetrahedral anions through 45° around their fourfold axis as facilitated by incorporation of dopants in the host lattice system [11, 37, 38].

5.3. Conclusion

Room temperature Raman spectra revealed internal stretching and bending vibrations of the tetrahedral as well as external mode signals of Eu^{3+}. Raman mode in the high-frequency regime corresponding to vibrational structure in free tetrahedral $[VO_4]^{3-}$ anionic group was found to be most intense among other modes observed. While the low frequency signal displayed highly asymmetrical profile upon varying Eu^{3+} concentration. Importantly, scheelite like characteristic overlap of two modes: A_{1g} (scissoring) and B_{2g} (twisting) was observed. Lattice distortions due to dopant induced crystal defect. and partial phase transformation has been elucidated. Partial zircon lattice to scheelite lattice can thus be facilitated as a rotation of the tetrahedral anions through 45° around their fourfold axis existence even at ambient conditions. Occupancy of irregular sites of the tetrahedral anion $[VO_4]^{3-}$ lead to shifting and widening observed with respect to

one another, thereby manifesting splitting due to change in crystal field upon doping. An attempt has been made to visualize the transition process with change in projections of the related hkl planes required for the phase change. The study can be extended with evaluation of temperature and pressure dependency on partial phase transition and its correlation with varying dopant concentration.

References

[1] Zagumennyi, A., Mikhailov, V., and Shcherbakov, I., Handbook of Laser Technology and Applications. 2004.

[2] Ivleva, L., Dunaeva, E., Voronina, I., Doroshenko, M., Papashvili, A., Sulc, J., Kratochvíl, J., and Jelinkova, H., Impact of Tm^{3+}/Ho^{3+} co-doping on spectroscopic and laser properties of $Ca_3(VO_4)_2$ single crystal. Journal of crystal growth, 513:10-14, 2019.

[3] Lu, G., Li, C., Wang, W., Wang, Z., Xia, H., and Zhao, P., Raman investigation of lattice vibration modes and thermal conductivity of Nd-doped zircon-type laser crystals. Materials Science and Engineering: B, 98(2):156-160, 2003.

[4] Wyss, C.P., Lüthy, W., Weber, H., Vlasov, V., Zavartsev, Y.D., Studenikin, P., Zagumennyi, A., and Shcherbakov, I., Performance of a diode-pumped 5 W Nd^{3+}: $GdVO_4$ microchip laser at 1.06 μm. Applied Physics B, 68(4):659-661, 1999.

[5] Kaminskii, A.A., Ueda, K.-i., Eichler, H.J., Kuwano, Y., Kouta, H., Bagaev, S.N., Chyba, T.H., Barnes, J.C., Gad, G.M., and Murai, T., Tetragonal vanadates YVO_4 and $GdVO_4$–new efficient χ (3)-materials for Raman lasers. Optics communications, 194(1-3):201-206, 2001.

[6] Frank, M., Smetanin, S.N., Jelínek, M., Vyhlídal, D., Ivleva, L.I., Dunaeva, E.E., Voronina, I.S., Tereshchenko, D.P., Shukshin, V.E., and Zverev, P.G., Stimulated Raman Scattering in Yttrium, Gadolinium, and Calcium Orthovanadate Crystals with Single and Combined Frequency Shifts under Synchronous Picosecond Pumping for Sub-Picosecond or Multi-Wavelength Generation around 1.2 μm. Crystals, 10(10):871, 2020.

[7] Lin, J. and Pask, H.M., Cascaded self-Raman lasers based on 382 cm^{-1} shift in Nd: $GdVO_4$. Optics Express, 20(14):15180-15185, 2012.

[8] Porto, S. and Scott, J., Raman Spectra of $CaWO_4$, $SrWO_4$, $CaMoO_4$, and $SrMoO_4$. Physical Review, 157(3):716, 1967.

[9] Zhang, C., Zhang, Z., Dai, R., Wang, Z., Zhang, J., and Ding, Z., High-pressure raman and luminescence study on the phase transition of GdVO4: Eu3+ microcrystals. The Journal of Physical Chemistry C, 114(42):18279-18282, 2010.

[10] Marqueño, T., Monteseguro, V., Cova, F., Errandonea, D., Santamaria-Perez, D., Bandiello, E., and Bettinelli, M., High-pressure phase transformations in NdVO4 under hydrostatic, conditions: a structural powder x-ray diffraction study. Journal of Physics: Condensed Matter, 31(23):235401, 2019.

[11] Voron'ko, Y.K., Sobol, A., Shukshin, V., Zagumennyĭ, A., Zavartsev, Y.D., and Kutovoĭ, S., Raman spectroscopic study of structural disordering in YVO_4, $GdVO_4$, and $CaWO_4$ crystals. Physics of the Solid State, 51(9):1886-1893, 2009.

[12] Guedes, I., Hirano, Y., Grimsditch, M., Wakabayashi, N., Loong, C.-K., and Boatner, L., Raman study of phonon modes in $ErVO_4$ single crystals. Journal of Applied Physics, 90(4):1843-1846, 2001.

[13] Elliott, R.J., Harley, R., Hayes, W., and Smith, S., Raman scattering and theoretical studies of Jahn—Teller induced phase transitions in some rare-earth compounds. Proceedings of the Royal Society of London. A. Mathematical and Physical Sciences, 328(1573):217-266, 1972.

[14] Santos, C., Silva, E., Ayala, A., Guedes, I., Pizani, P., Loong, C.-K., and Boatner, L.A., Raman investigations of rare earth orthovanadates. Journal of Applied Physics, 101(5):053511, 2007.

[15] Pellicer-Porres, J., Vazquez-Socorro, D., López-Moreno, S., Muñoz, A., Rodríguez-Hernández, P., Martínez-García, D., Achary, S., Rettie, A.J., and Mullins, C.B., Phase transition systematics in $BiVO_4$ by means of high-pressure–high-temperature Raman experiments. Physical Review B, 98(21):214109, 2018.

[16] Jovanović, D.J., Chiappini, A., Zur, L., Gavrilović, T.V., Tran, T.N.L., Chiasera, A., Lukowiak, A., Smits, K., Dramićanin, M.D., and Ferrari, M., Synthesis, structure and spectroscopic properties of luminescent $GdVO_4$:Dy^{3+} and $DyVO_4$ particles. Optical Materials, 76:308-316, 2018.

[17] Zverev, P.G., Karasik, A.Y., Basiev, T.T., Ivleva, L.I., and Osiko, V.V., Stimulated Raman scattering of picosecond pulses in $SrMoO_4$ and $Ca_3(VO_4)_2$ crystals. Quantum Electronics, 33(4):331, 2003.

[18] Basiev, T., Vassiliev, S., Konjushkin, V., Osiko, V., Zagumennyi, A., Zavartsev, Y., Kutovoi, S., and Shcherbakov, I., Diode pumped 500-picosecond Nd: $GdVO_4$ Raman laser. Laser physics letters, 1(5):237, 2004.

[19] Huang, G., Yu, Y., Xie, X., Zhang, Y., and Du, C., Diode-pumped simultaneously Q-switched and mode-locked YVO_4/Nd:YVO_4/YVO_4 crystal self-Raman first-Stokes laser. Optics express, 21(17):19723-19731, 2013.

[20] Grzechnik, A., Local structures in high pressure phases of V2O5. Chemistry of materials, 10(9):2505-2509, 1998.

[21] Thakur, H., Singh, R.K., and Gathania, A.K., Synthesis and optical properties of GdVO4: Eu3+ phosphor. Materials Research Express, 8(2):026201, 2021.

[22] Bai, F., Jiao, Z., Xu, X., and Wang, Q., High power Stokes generation based on a secondary Raman shift of 259 cm− 1 of Nd: YVO_4 self-Raman crystal. Optics & Laser Technology, 109:55-60, 2019.

[23] IA, B., Vinogradova, N., Dem'yanets, L., Ezhova, Z.A., Ilyukhin, V., Kara-Ushanov, V.Y., Komissarova, L., Lazarevskiœ, E., Livitin, B., and Mel'nikov, P., Compounds of Rare-Earth Elements: Silicates, Germanates, Phosphates, Arsenates, and Vanadates. 1983.

[24] Pal, M., Pal, U., Jiménez, J.M.G.Y., and Pérez-Rodríguez, F., Effects of crystallization and dopant concentration on the emission behavior of TiO_2:Eu nanophosphors. Nanoscale research letters, 7(1):1-12, 2012.

[25] Tuschel, D., Effect of dopants or impurities on the raman spectrum of the host crystal. Spectroscopy, 32:13-18, 2017.

[26] Ningthoujam, R., Vatsa, R., Pandey, M., Shanta Singh, N., Dorndrajit Singh, S., and Yaiphaba, N. Raman studies of Eu^{3+} doped $GdVO_4$. in Proceedings of second DAE-BRNS international symposium on materials chemistry. 2008.

[27] Lazarev, A., Mirgorodskiy, A., and Mazhenov, N., Resonance interactions of the localized vibrators in crystals of ABO_4-type: vibration spectra of crystals with zircon and xenotime structures. The Vibration of Oxide Lattices. Nauka, Leningrad, 72:99, 1980.

[28] Brooker, M., Raman evidence for thermally disordered energy states in various phases of ionic nitrates. The Journal of Chemical Physics, 68(1):67-73, 1978.

[29] Gouadec, G. and Colomban, P., Raman Spectroscopy of nanomaterials: How spectra relate to disorder, particle size and mechanical properties. Progress in crystal growth and characterization of materials, 53(1):1-56, 2007.

[30] Khosravi Ghandomani, S., Khoshnevisan, B., and Yousefi, R., The capability of SnTe QDs as QDSCs working in the visible–NIR region and the effects of Eu-doping on improvement of solar cell parameters. Journal of Materials Science: Materials in Electronics, 29(22):18989-18996, 2018.

[31] Miranda, G.G., e Silva, R.L.d.S., dos Santos Pessoni, H.V., and Franco Jr, A., Raman spectroscopy study of Ga-doped ZnO ceramics: An estimative of the structural disorder degree. Physica B: condensed matter, 606:412726, 2021.

[32] Huang, Y., Liu, M., Li, Z., Zeng, Y., and Liu, S., Raman spectroscopy study of ZnO-based ceramic films fabricated by novel sol–gel process. Materials Science and Engineering: B, 97(2):111-116, 2003.

[33] Flórez, M., Contreras-García, J., Recio, J., and Marques, M., Quantum-mechanical calculations of zircon to scheelite transition pathways in $ZrSiO_4$. Physical Review B, 79(10):104101, 2009.

[34] Schustereit, T., Müller, S.L., Schleid, T., and Hartenbach, I., Defect scheelite-type lanthanoid (III) ortho-oxomolybdates (VI) $Ln_{0.667}$ [MoO_4] (Ln= Ce, Pr, Nd, and Sm) and their relationship to zircon and the NaTl-type structure. Crystals, 1(4):244-253, 2011.

[35] Long, Y., Liu, Q., Lv, Y., Yu, R., and Jin, C., Various 3*d*-4*f* spin interactions and field-induced metamagnetism in the Cr^{5+} system $DyCrO_4$. Physical Review B, 83(2):024416, 2011.

[36] Kusaba, K., Yagi, T., Kikuchi, M., and Syono, Y., Structural considerations on the mechanism of the shock-induced zircon-scheelite transition in $ZrSiO_4$. Journal of Physics and Chemistry of Solids, 47(7):675-679, 1986.

[37] Jayaraman, A., Kourouklis, G., Espinosa, G., Cooper, A., and Van Uitert, L., A high-pressure Raman study of yttrium vanadate (YVO_4) and the pressure-induced transition from the zircon-type to the scheelite-type structure. Journal of Physics and Chemistry of Solids, 48(8):755-759, 1987.

[38] Knittle, E. and Williams, Q., High-pressure Raman spectroscopy of $ZrSiO_4$: Observation of the zircon to scheelite transition at 300 K. American Mineralogist, 78(3-4):245-252, 1993.